catalysts

MDPI

Article

A Study on Electron Acceptor of Carbonaceous Materials for Highly Efficient Hydrogen Uptakes

Seul-Yi Lee [1,2,3], Ji-Hye Park [1], Young-Jung Heo [1], Eun-Sang Lee [3,4] and Soo-Jin Park [1,*]

[1] Department of Chemistry, Inha University, Incheon 22212, Korea; leesy1019@inha.ac.kr (S.-Y.L.); pjihye9874@gmail.com (J.-H.P.); heoyj1211@naver.com (Y.-J.H.)
[2] Department of Mechanical Engineering, Institute for Critical Technology and Applied Science, Virginia Tech, Blacksburg, VA 24061, USA
[3] KIURI Center for Hydrogen Based Next Generation Mechanical System, Incheon 21999, Korea; leees@inha.ac.kr
[4] Department of Mechanical Engineering, Inha University, Incheon 22212, Korea
* Correspondence: sjpark@inha.ac.kr; Tel.: +82-32-876-7234

Abstract: Significant efforts have been directed toward the identification of carbonaceous materials that can be utilized for hydrogen uptake in order to develop on-board automotive systems with a gravimetric capacity of 5.5 wt.%, thus meeting the U.S. Department of Energy technical targets. However, the capacity of hydrogen storage is limited by the weak interaction between hydrogen molecules and the carbon surface. Cigarette butts, which are the most abundant form of primary plastic waste, remain an intractable environmental pollution problem. To transform this source of waste into a valuable adsorbent for hydrogen uptake, we prepared several forms of oxygen-rich cigarette butt-derived porous carbon (CGB-AC, with the activation temperature range of 600 and 900 °C). Our experimental investigation revealed that the specific surface area increased from 600 to 700 °C and then decreased as the temperature rose to 900 °C. In contrast, the oxygen contents gradually decreased with increasing activation temperature. CGB-AC700 had the highest H_2 excess uptake (Q_{Excess}) of 8.54 wt.% at 77 K and 20 bar, which was much higher than that of porous carbon reported in the previous studies. We found that the dynamic interaction between the porosity and the oxygen content determined the hydrogen storage capacity. The underlying mechanisms proposed in the present study would be useful in the design of efficient hydrogen storage because they explain the interaction between positive carbonaceous materials and negative hydrogen molecules in quadrupole orbitals.

Keywords: hydrogen storage; oxygen-functional groups; porous carbons; pore size; 77 K

Citation: Lee, S.-Y.; Park, J.-H.; Heo, Y.-J.; Lee, E.-S.; Park, S.-J. A Study on Electron Acceptor of Carbonaceous Materials for Highly Efficient Hydrogen Uptakes. *Catalysts* **2021**, *11*, 1524. https://doi.org/10.3390/catal11121524

Academic Editor: Consuelo Alvarez-Galvan

Received: 16 November 2021
Accepted: 14 December 2021
Published: 15 December 2021

1. Introduction

For several decades, fossil fuels have been the primary energy source for industrial activity. However, the combustion of fossil fuels results in pollutant emissions and contributes to a wide variety of environmental problems including global warming and climate change. Therefore, clean and sustainable alternative energy sources such as wind, biomass, waves, and natural gas are required. In this respect, hydrogen (H_2) has emerged as a promising renewable energy source for reducing the dependence on fossil fuels, thus leading to the development of a hydrogen economy [1–4].

One of the current drawbacks of utilizing H_2 is the lack of safe and economical storage systems [5,6]. Existing H_2 storage methods such as compressed gas and liquefied H_2 are complex due to the fact that H_2 has a low boiling point (20 K) and a low density (0.08988 g/L) at ambient pressure. Compressed gas requires very high pressures, meaning costly additional equipment is required to achieve the capacity required for practical use, while liquefied H_2 requires cryogenic temperatures and additional refrigeration, which can lead to vaporization and the loss of H_2. Due to these disadvantages, both storage methods have safety problems [7–9]. The U.S. Department of Energy (DOE) has established H_2

storage technical targets for the gravimetric capacity (5.5 wt.%) and volumetric capacity (30 g/L) of on-board automotive systems to be achieved by 2025. In order to reach these targets, physisorption has attracted significant attention as a promising method for H_2 storage because of its reversibility, fast kinetics, and high H_2 uptake [10–13].

Storage materials have been extensively investigated for efficient H_2 physisorption including carbon materials [14–16], metal organic frameworks (MOFs) [17–20], and zeolites [21–23]. Porous carbon materials including activated carbon (AC) have proven to be particularly promising adsorbents due to their high specific surface area (SSA), high porosity, and chemical and thermal stabilities [24,25]. It is also well-known that chemical activation using activating reagents such as potassium hydroxide (KOH), sodium hydroxide (NaOH), and zinc chloride ($ZnCl_2$) for the preparation of AC can lead to additional advantages such as a higher SSA, improved microporosity, and low-temperature pyrolysis [26–29].

Several studies have reported that a high SSA is a key characteristic required to maximize the amount of H_2 adsorbed onto AC [30,31]. However, the high H_2 uptake of AC depends not only on the SSA, but also on its surface characteristics, which affect the interaction between H_2 molecules and the carbon surface. The surface functionalization of AC can help to improve this interaction and promote the high storage performance of H_2. However, it has been reported that surface functionalization alters the surface characteristics of AC and decreases the porosity due to the introduction of foreign functional groups [32]. The key to overcoming these issues is identifying appropriate precursors for the development of AC. For optimal use as a H_2 storage material, AC should have a high SSA with well-developed micropores and precursors should have desirable surface properties that are retained in the resulting AC.

Many attempts have been made to understand the effect of oxygen-functional groups on the surface of carbonaceous materials for H_2 uptake behaviors [33]. Some researchers have reported that oxygen functional groups on AC decrease its H_2 storage capacity due to steric hindrance in the pores and an increase in the solid [34]. However, contradictory experimental results have shown that oxygen functional groups on AC can significantly increase H_2 storage capacity, acting as active adsorption sites for H_2 molecules. This outcome can also be explained by the influence of the acidic oxygen functional groups on the physisorption energy, which can be defined by the Dubinin–Astakhov model or electron acceptor–donor interactions at the carbon surface [35–37]. In order to resolve these conflicting observations, it is vital to explain the interaction between the oxygen functional groups and the textural properties of AC; this information could then be employed to maximize H_2 storage capacity.

An estimated 5.7 trillion cigarette butts (CGBs) are disposed of globally as litter each year, and these contain contaminants that can be harmful to the environment and humans [36]. For this reason, CGBs need to be disposed of in an environmentally friendly manner, and their use as a precursor for value-added processes could be a useful strategy to achieve this. CGBs are mainly composed of cellulose acetate, which can be used as a carbon precursor with significant oxygen content [38,39]. Mokaya et al. investigated the potential of oxygen-rich activated carbons and reported that the H_2 storage capacity exhibited excess hydrogen uptakes between 4.6 and 7.0 wt.% at 77 K and 20 bar due to the combined effects of high surface area, high microporosity, and an oxygen-rich nature [39,40].

Here, we investigated the use of CGBs as a carbon precursor for H_2 storage capacities. The aim of this study was to investigate the relationship between the oxygen content and the textural properties of CGB-AC, and further the resulting effect on their H_2 storage behaviors by the electron acceptor–donor interaction between oxygen moieties and hydrogen molecules. From the experimental results, CGB-AC700 (i.e., AC prepared at 700 °C), with a SSA of 2850 m^2/g, had the highest H_2 storage capacity (8.54 wt.% at 77 K and 20 bar). This can primarily be attributed to the porosity. We also found that the oxygen content of the CGB-AC provided effective adsorption sites, resulting in improvement of H_2 uptake.

2. Results and Discussion

2.1. Synthesis and the Morphology

CGBs as a carbon precursor were initially carbonized using a hydrothermal reaction to obtain CGB-*d*-hydrochar. Chemical activation was then conducted using KOH to induce porosity in the CGB-*d*-hydrochar. The pore structure of the CGB-*d*-hydrochar was produced via KOH activation using an etching carbon framework and redox reactions with potassium compounds. The following reactions explain this mechanism [41]:

$$4KOH + C \rightarrow K_2CO_3 + K_2O + 2H_2,$$

$$2KOH \rightarrow K_2O + H_2O,$$

$$C + H_2O \rightarrow H_2 + CO,$$

$$CO + H_2O \rightarrow H_2 + CO_2,$$

$$K_2O + CO_2 \rightarrow K_2CO_3,$$

$$H_2O + H_2 \rightarrow 2K + H_2O,$$

$$K_2O + C \rightarrow 2K + CO,$$

$$K_2CO_3 + 2C \rightarrow 2K + 3CO.$$

In these reactions, the porous structure was created by oxidizing the carbon atoms. Scanning electron microscopy (SEM) images of CGB-*d*-hydrochar and CGB-AC samples produced at different activation temperatures are presented in Figure 1a–e. In Figure 1a, the CGB-*d*-hydrochar exhibited a smooth, non-porous surface. After KOH activation, pores were observed on the carbon surface. With an increasing activation temperature, the pores became larger and larger craters appeared at temperatures above 800 °C (Figure 1b–e), which indicated the collapse of the porous structure.

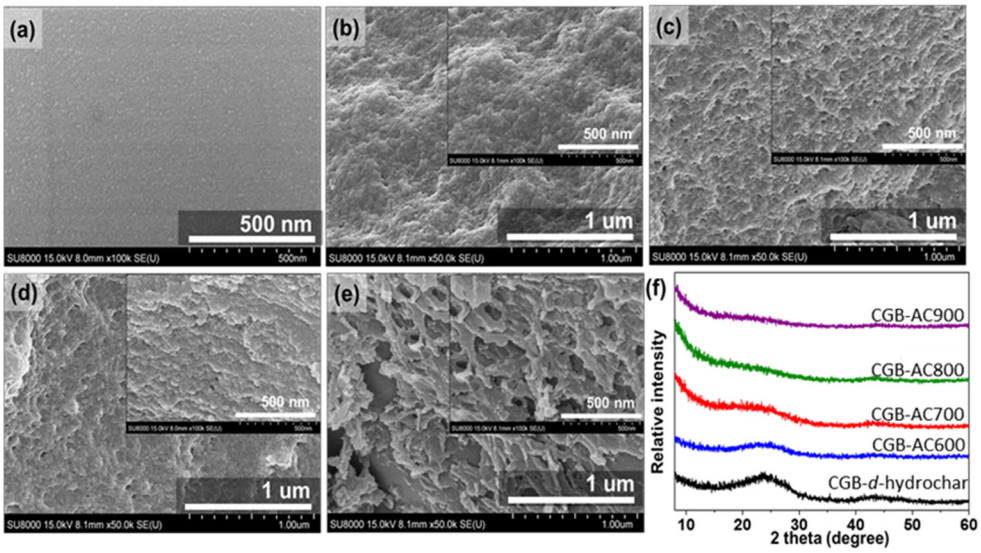

Figure 1. SEM images of (**a**) CGB-*d*-hydrochar and (**b**–**e**) CGB-AC samples at different activation temperatures ((**b**): 600 °C, (**c**): 700 °C, (**d**): 800 °C, and (**e**): 900 °C), and (**f**) XRD patterns for the obtained samples.

2.2. Structural Properties

X-ray diffraction (XRD) patterns for the CGB-*d*-hydrochar and CGB-AC samples are presented in Figure 1f. Broad peaks at 2θ = 23.5° (1 0 1) and 44° (1 0 0, 1 0 1) were observed for the CGB-*d*-hydrochar, indicating an amorphous graphitic structure consisting of randomly distributed carbon [42]. The peaks at 2θ = 23.5° and 44° in the CGB-AC

samples decreased with higher activation temperatures due to an increase in the irregularity of the graphitic structure and its eventual collapse, which was in agreement with the SEM results [43].

2.3. Elemental Compositions

The elemental composition of the prepared samples is displayed in Table 1. The O content of CGB-*d*-hydrochar was 41.8%, while that of the CGB-AC samples was 18.5–38.5%, higher than the typical range for AC derived from cellulose-derived polymeric precursors (~11%) [40,44,45]. This indicates that the CGB-AC samples had a high concentration of O, which may be attributable to the oxygen moieties produced from the CGB-*d*-hydrochar during the activation process. It was expected that the relative content of C in the hydrochar would increase gradually with an increasing KOH activation temperature while that of O would decrease [46]. However, the relative atomic content of H gradually declined while that of O decreased less dramatically. This might be because the aliphatic compounds in CGB-*d*-hydrochar were preferentially removed during the activation process. In particular, the CGB-AC600 and CGB-AC700 samples retained a high O content of 38.5% and 37.9%, respectively. The CGB-*d*-hydrochar and CGB-AC samples also contained low N content, which was attributable to the nicotine from smoking.

Table 1. Elemental analysis of the CGB-*d*-hydrochar and CGB-AC samples.

Samples	C (%)	H (%)	O (%)	N (%)	O/C	H/C
CGB-*d*-hydrochar	50.3	6.7	41.8	1.2	0.831	0.133
CGB-AC600	59.7	0.8	38.5	1.0	0.645	0.013
CGB-AC700	62.0	0.5	37.9	0.6	0.611	0.008
CGB-AC800	74.6	0.6	24.3	0.5	0.326	0.008
CGB-AC900	80.4	0.4	18.5	0.7	0.230	0.004

2.4. Surface Properties

To further explore the behaviors of the oxygen functional groups in the CGB-*d*-hydrochar and CGB-AC samples, we carried out Fourier transform infrared (FTIR) and X-ray photoelectron spectroscopy (XPS) measurements. The FTIR spectra of the prepared samples are presented in Figure S1, showing a broad peak at 3400 cm^{-1} corresponding to the O–H stretching vibrations from the hydroxyl or carboxyl groups, which decreased with an increase in the activation temperature [47]. The prepared samples exhibited a wide band at 2800–3000 cm^{-1} attributable to the C–H band for alkyl groups, which is generally found in all carbon materials at varying peak intensities [48]. Moreover, the prominent peak corresponding to C=O stretching vibrations at 1620 cm^{-1} indicated that the CGB-AC samples had various oxygen functional groups [47]. It is also important that the peaks for the oxygen functional groups in the CGB-*d*-hydrochar were higher than those for the CGB-AC samples, which corresponded with the elemental analysis results.

The XPS spectra were recorded at a range of 200–700 eV, as shown in Figure S2. The spectra exhibited two prominent peaks at a binding energy of 531 and 284.5 eV, corresponding to O1s and C1s, respectively [49]. The prominent peaks for O1s in all samples indicated that abundant oxygen functional groups remained at the CGB-AC surfaces during the thermal activation process [50]. It was clearly observed that the peak intensity of O1s decreased while that of C1s increased with an increase in the activation temperature.

2.5. Textural Properties

The textural properties of the CGB-AC samples were verified using their nitrogen adsorption–desorption isotherms at 77 K, as presented in Figure 2a and Table 2. The CGB-AC samples exhibited typical Type I isotherms, in accordance with the IUPAC classification, which is characteristic of microporous materials based on a sharp increase in the amount of N_2 adsorbed at very low relative pressures below 0.1 [51]. We found that the SSA and total

pore volume increased following KOH activation at increasing activation temperatures up to 700 °C and then decreased abruptly. It was expected that the KOH activation would promote the development of a porous structure, especially micropores, resulting in more advantageous textural properties [52]. The porosity was the highest for the CGB-AC700 sample, which exhibited the highest SSA and V_{total} (2850 m^2/g and 1.734 cm^3/g, respectively).

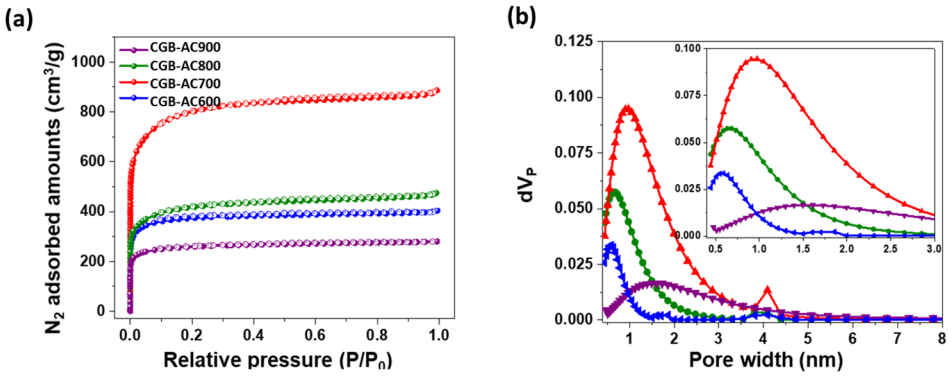

Figure 2. (**a**) N_2 adsorption–desorption isotherms of CGB-AC samples recorded at 77 K and (**b**) pore size distributions of the prepared samples as determined using the NLDFT method.

Table 2. Textural properties and hydrogen uptake of the CGB-AC samples.

Samples	[a] SSA (m^2 g^{-1})	[b] V_{total} (cm^3 g^{-1})	[c] V_{micro} (cm^3 g^{-1})	[d] V_{meso} (cm^3 g^{-1})	[e] F_{micro} (%)	H_2 Uptake (wt.%) [f] Q_{excess}	[g] Q_{total}
CGB-AC600	1412	0.858	0.834	0.023	97.20	5.79	5.85
CGB-AC700	2850	1.734	1.559	0.175	89.91	8.54	9.67
CGB-AC800	1520	1.156	1.028	0.128	88.93	3.27	4.05
CGB-AC900	987	0.516	0.490	0.026	94.96	2.40	2.74

[a] SSA: specific surface area computed using BET equation at a relative pressure range of 0.00001–0.01; [b] V_{total}: total pore (0–50 nm) volume determined from the NLDFT method; [c] V_{micro}: micropore (0–2 nm) volume determined from the NLDFT method; [d] V_{meso}: mesopore (2–50 nm) volume determined from the NLDFT method; [e] F_{micro}: fraction of micropore volume = (micropore volume/total pore volume) × 100; [f] Q_{excess}: H_2 excess uptakes at 77 K and 20 bar; [g] Q_{total}: H_2 total uptakes at 77 K and 20 bar.

The decrease in the N_2/77 K adsorption–desorption isotherms for the CGB-AC800 and CGB-AC900 samples indicated that a KOH activation temperature above 800 °C caused the porous structure to collapse. This is linked to the results for the pore size distribution (PSD) results (Figure 2b). The PSD for the CGB-AC samples had a broad peak at a pore size range of 0.5–3.0 nm, with the CGB-AC700 sample exhibiting a more dominant peak at 1 nm compared to the other samples, which is indicative of the presence of a well-developed microporous structure. For the CGB-AC800 and CGB-AC900 samples, the peak intensity decreased dramatically with an increase in the activation temperature, with CGB-AC900 exhibiting a broad peak at a comparably larger pore size range of 0.5–4.0 nm. This represents clear evidence that the porous structure was destroyed as the pores merged into wider pores at a higher activation temperature above 800 °C.

2.6. Hydrogen Adsorption Behaviors

The overall adsorption isotherms are presented in Figure 3. The excess adsorption (Q_{excess}) and the absolute amount of gas adsorbed (Q_{total}) for H_2 at 77 K and 20 bar are also summarized in Table 2. Q_{total} was determined while experiments measured Q_{excess}. These values were obtained using Equation (1) [53]:

$$Q_{excess} = Q_{total} - V_{pore}\rho_{bulk}\ (P, T) \quad (1)$$

where V_{pore} is the total pore volume for the adsorbent and ρ_{bulk} is the density of the bulk gas (i.e., H_2) at the given adsorption pressure and temperature. The bulk H_2 density at

different pressures was obtained from the National Institute of Standards and Technology (NIST) [54].

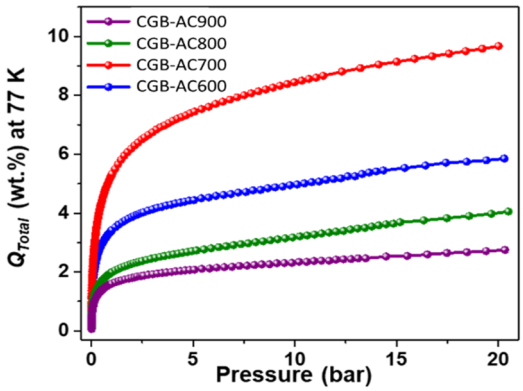

Figure 3. Total H_2 storage capacity of CGB-AC samples at 77 K and 20 bar.

Based on Equation (1), CGB-AC700 had the highest Q_{total} (9.67 wt.%) at 77 K and 20 bar. The high SSA and microporosity of the CGB-AC700 sample increased its H_2 storage capacity because of the higher number of H_2 adsorption sites. Similarly, the hydrogen uptake was lowest for CGB-AC900 (2.40 wt.%) because of its low porosity.

Normally, the hydrogen adsorption capacity of activated carbons with high SSA tends to be in line with Chahine's rule. Chahine's rule is a typical trend obtained empirically where approximately 1 wt.% of gravimetric H_2 uptake is obtained for every 500 m^2 g^{-1} of SSA at 77 K and elevated pressure up to ~350 bar [55,56]. Figure 4a displays Chahine's line (solid) and the relationship between Q_{excess} and SSA for CGB-AC samples. We found that CGB-AC800 and CGB-AC900 samples were closely related to the SSA while the others (CGB-AC600 and CGB-AC700) greatly outperformed at the trend. This exceptionally high H_2 uptake of CGB-AC600 and CGB-AC700 might be attributed to the high oxygen contents of 38.5% and 37.9%, respectively, on the carbon surfaces [40].

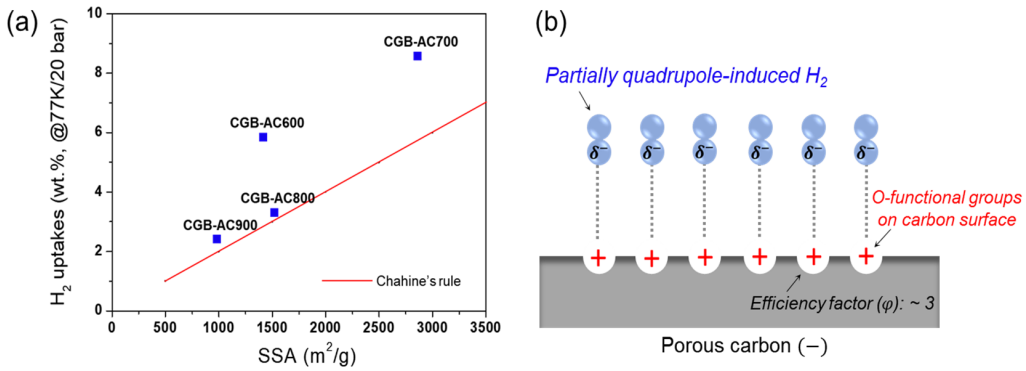

Figure 4. (**a**) Relationship between H_2 uptake capacity and specific surface area for CGB-AC samples and (**b**) schematic illustration of the oxygen-rich porous carbon surface of CGB-AC and the adsorption mechanism of partially quadrupole-induced H_2 molecules.

The H_2 uptake of CGB-AC700 was much higher than that reported for other experimental results in the literature when using carbon materials with a similar range of textural properties under the same conditions (6.5–7 wt.%) [44,57–62]. The CGB-AC samples in the present study had a higher oxygen content, suggesting that the oxygen levels of carbon materials may influence their H_2 storage behaviors. It was also found that the Q_{total} for CGB-AC800 was lower than that of CGB-AC600 (4.06 wt.% and 5.85 wt.%, respectively) even though they had similar textural properties. The oxygen content of CGB-AC600 was higher than that of CGB-AC800, providing more evidence that oxygen functional play a

key role in improving the electron acceptor characteristics (δ^+) of the material, resulting in increasing the H_2 (δ^-) uptake (Figure 4b).

Our experimental results revealed that the synergetic effect between the textural properties and the oxygen content is a significant factor in improving H_2 uptake. The Q_{excess} of the CGB-AC samples was between 2.40 wt.% and 8.54 wt.%, leading to a Q_{total} of between 2.74 wt.% and 9.67 wt.%. It was also remarkable that a Q_{total} greater than 7.67 wt.% was observed above 20 bar of Q_{total} for any of the samples. These results can be explained in relation to the surface interactions of polar and nonpolar adsorbates. With a polar adsorbate, the electron acceptor–donor interaction plays a dominant role in hydrogen adsorption. Figure 4b presents the effect of oxygen functional groups on the carbon surface for H_2 adsorption, suggesting that oxygen functional groups provide H_2-affiliated sites. These acidic sites are charged, thus polarizing the H_2 molecules [63]. Although a direct charge transfer does not occur between H_2 molecules and the oxygen functional groups, the charge-induced dipole interaction offers adsorption-friendly sites in accordance with a partial loss of positively charged electrons, which is associated with the strong electron-acceptor characteristics [63]. In contrast, for a nonpolar adsorbate, the effect of pore size is dominant. Thus, an optimized pore size would be important for efficient H_2 physisorption. The efficiency factor (φ) for pore size in an effective H_2 physisorption process can be estimated using experimental and theoretical calculations, as described in Equation (2):

$$\varphi = \frac{\text{Effective pore size}}{\text{Kinetic diameter of } H_2 \text{ molecule}} \quad (2)$$

where the kinetic diameter of H_2 molecules is 0.289 nm and the effective pore size represents a variable optimum pore size.

In a previous study, we experimentally determined that the φ of activated multi-walled carbon nanotubes (A-MWCNTs) prepared using KOH activation was approximately 2.5 at 77 K and 1 bar [64]. It can be assumed that much effective hydrogen uptake can be observed in the efficiency factor of 2.5. In the present study, the efficiency factor (φ) fits roughly within a larger range, and it is clearly presented that the factors in the range of 2.0 to 3.1 showed quite a high value of Q_{total} in the CGB-AC600, 700, and 800 samples, while CGB-AC900 showed the lowest Q_{total} because it was far off the factor of 5.1.

Detailed information on the surface characteristics of the CGB-AC samples is critical to understanding their observed H_2 storage behavior. As listed in Table 3, the φ for CGB-AC600 and CGB-AC800 was 2.0 and 2.1, respectively, but they exhibited a different Q_{total}, possibly due to the much higher oxygen content in CGB-AC600. In addition, for CGB-AC700, which had the highest Q_{total}, the estimated φ was ~3, which was a result of its highest peak intensity in the PSD analysis, occurring at approximately 0.9 nm. It is important to note that φ can be affected by variation in the pressure and temperature. The closer φ is to 3, the more efficient it is for H_2 adsorption using carbonaceous materials at 77 K and 20 bar in the presence of higher oxygen content. Thus, CGB-AC700 exhibited an exceptional Q_{Excess} of 8.54 wt.% at 77 K and 20 bar when compared to previous studies. Consequently, we suggest that the interaction between the adsorbate based on its electron-donor polarity (δ^-) and the adsorbent based on its electron-acceptor polarity (δ^+) should be considered in the design of a highly efficient H_2 adsorption system.

Table 3. Peak centers from pore size distribution analysis and the efficiency factor (φ) for hydrogen uptake for the CGB-AC samples.

Samples	Peak Center (nm)	Efficiency Factor (φ)
CGB-AC600	0.59	2.0
CGB-AC700	0.90	3.1
CGB-AC800	0.63	2.1
CGB-AC900	1.49	5.1

3. Experimental Section

3.1. Sample Preparation

Littered cigarette butts (CGB) were collected to use as a precursor. Prior to the experiment, the paper wrapped around the CGB was removed, and then the CGBs were ground using a mortar. Hydrothermal carbonization was then performed to obtain CGB-derived hydrochar (CGB-*d*-hydrochar). The synthetic route for the CGB-*d*-AC (hereafter CGB-AC) is presented in Scheme 1. The ground CGBs were heated in a stainless-steel autoclave at 250 °C at a heating rate of 5 °C/min, followed by cooling to room temperature. The synthesized CGB-*d*-hydrochar was mixed with KOH (at a KOH/CGB-*d*-hydrochar weight ratio of 5 for chemical activation. A tubular furnace was heated to the target temperature at a heating rate of 5 °C/min and maintained for 1 h in a nitrogen atmosphere. The obtained CGB-AC was then washed with distilled water until a neutral pH was observed, followed by drying in an oven at 80 °C for 24 h. The prepared CGB-AC samples were labelled CGB-AC'T', where T indicates the activation temperature.

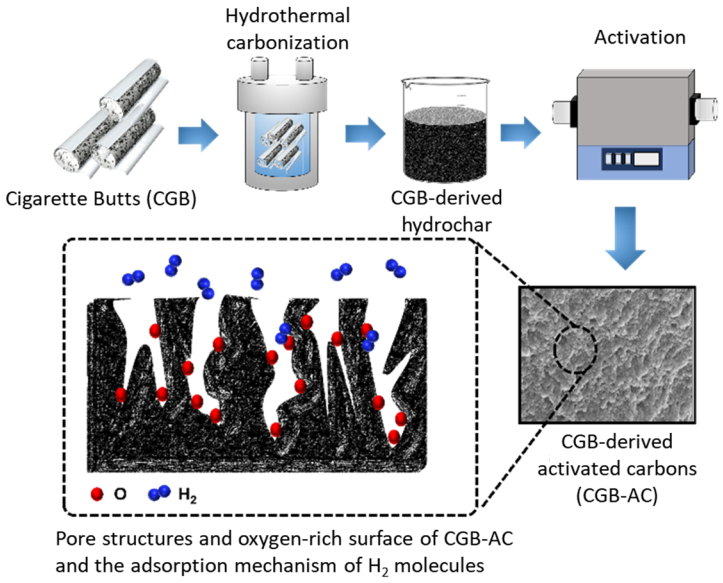

Scheme 1. Schematic illustration of the preparation process for CGB-AC samples.

3.2. Characterization and Hydrogen Adsorption Measurement

The morphology of the samples was investigated using scanning electron microscopy (SEM, Model SU 8010, Hitachi Co., Japan). The surface characteristics of the prepared samples were examined by X-ray photoelectron spectroscopy (XPS, K-Alpha, Thermo Scientific Co., USA), and the functional groups on the prepared samples were observed with a Fourier transform-infrared vacuum spectrometer (FT-IR, VERTEX 80V, Bruker Co., Germany). An elemental analyzer (EA, EA1112, Thermo Scientific Co.) was used to investigate the chemical elemental composition of the prepared samples. The textural properties of the samples were obtained from nitrogen adsorption–desorption isotherms at 77 K with a volumetric adsorption analyzer (Belsorp Max, BEL Japan Inc., Japan). The SSA was calculated using the Brunauer–Emmett–Teller (BET) equation, and the non-local density functional theory (NLDFT) was used to determine the pore size distribution (PSD). The H_2 adsorption isotherm was obtained using the volumetric analysis method using a gas adsorption analyzer (Model BEL-HP, BEL Japan, Inc., Japan) at 77 K and 20 bar. All of the samples were degassed before analysis at 473 K for 12 h in a vacuum. For the adsorption analysis, ultrahigh-purity H_2 (99.9999%) was used to eliminate the influence of impurities.

4. Conclusions

We prepared hydrothermally carbonized CGB-*d*-hydrochar with a high oxygen content. The CGB-*d*-hydrochar was chemically activated using KOH to obtain a highly porous carbon material. The resulting samples had varying oxygen levels and different textural properties, which resulted in a Q_{total} range of 2.74–9.67 wt.%. Our experimental data confirmed that the textural properties of the CGB-AC samples influenced their H_2 storage behavior. In particular, we found that the efficiency factor (φ) for H_2 molecules plays a key role in enhancing the H_2 uptake at 77 K and 20 bar. It was demonstrated that high oxygen levels in a carbon material play an important role in improving the electron acceptor–donor intermolecular interaction between the oxygen functional groups and H_2 molecules. Therefore, our experimental results for H_2 adsorption based on the φ of the pore size of the material should help in the design of more efficient H_2 uptake systems.

Supplementary Materials: The following are available online at https://www.mdpi.com/article/10.3390/catal11121524/s1, Figure S1: FTIR spectra of CGB-*d*-hydrochar and CGB-AC samples; Figure S2: The XPS survey scans of CGB-*d*-hydrochar and CGB-AC samples. Figure S3: Total H_2 uptakes of CGB-AC samples at 77 K and 20 bar.

Author Contributions: Conceptualization, S.-Y.L. and J.-H.P.; Data curation, J.-H.P. and Y.-J.H.; Investigation, Y.-J.H.; Project administration, and S.-J.P.; Writing—original draft, S.-Y.L. and S.-J.P.; Writing—review & editing, S.-Y.L., E.-S.L. and S.-J.P. All authors have read and agreed to the published version of the manuscript.

Funding: This work was supported by the Technology Innovation Program (or Industrial Strategic Technology Development Program), Innovative technology for CO_2 free hydrogen production using molten catalysts (20012373) funded by the Ministry of Trade, Industry & Energy(MOTIE, Korea), the Korea Electric Power Corporation (Grant number: R21XO01-5), and the Korea Initiative for Fostering University of Research and Innovation (KIURI) Program of the National Research Foundation (NRF) funded by the Korean government (MSIT) (No. NRF-2021M3H1A106413511).

Conflicts of Interest: The authors declare no conflict of interest.

References

1. Schlapbach, L.; Züttel, A. Hydrogen-storage materials for mobile applications. *Nature* **2001**, *414*, 353–358. [CrossRef] [PubMed]
2. Schoedel, A.; Ji, Z.; Yaghi, O.M. The role of metal–organic frameworks in a carbon-neutral energy cycle. *Nat. Energy* **2016**, *1*, 16034. [CrossRef]
3. Liu, C.; Fan, Y.Y.; Liu, M.; Cong, H.T.; Cheng, H.M.; Dresselhaus, M.S. Hydrogen storage in single-walled carbon nanotubes at room temperature. *Science* **1999**, *286*, 1127–1129. [CrossRef]
4. Browning, D.J.; Gerrard, M.L.; Lakeman, J.B.; Mellor, I.M.; Mortimer, R.J.; Turpin, M.C. Studies into the Storage of Hydrogen in Carbon Nanofibers: Proposal of a Possible Reaction Mechanism. *Nano Lett.* **2002**, *2*, 201–205. [CrossRef]
5. Zhao, X.B.; Xiao, B.; Fletcher, A.J.; Thomas, K.M. Hydrogen Adsorption on Functionalized Nanoporous Activated Carbons. *J. Phys. Chem. B* **2005**, *109*, 8880–8888. [CrossRef]
6. Latroche, M.; Surblé, S.; Serre, C.; Mellot-Draznieks, C.; Llewellyn, P.L.; Lee, J.H.; Chang, J.S.; Jhung, S.H.; Férey, G. Hydrogen storage in the giant-pore metal-organic frameworks MIL-100 and MIL-101. *Angew. Chem.* **2006**, *45*, 8227–8231. [CrossRef] [PubMed]
7. Thomas, K.M. Hydrogen adsorption and storage on porous materials. *Catal. Today* **2007**, *120*, 389–398. [CrossRef]
8. Sakintuna, B.; Lamari-Darkrim, F.; Hirscher, M. Metal hydride materials for solid hydrogen storage: A review. *Int. J. Hydrogen Energy* **2007**, *32*, 1121–1140. [CrossRef]
9. Eberle, U.; Arnold, G.; von Helmolt, R. Hydrogen storage in metal–hydrogen systems and their derivatives. *J. Power Sources* **2006**, *154*, 456–460. [CrossRef]
10. Choi, Y.K.; Park, S.J. Preparation and characterization of sucrose-based microporous carbons for increasing hydrogen storage. *J. Ind. Eng. Chem.* **2015**, *28*, 32–36. [CrossRef]
11. Ozturk, Z. Hydrogen storage on lithium modified silica based CHAbazite type zeolite, A computational study. *Int. J. Hydrogen Energy* **2018**, *43*, 22365–22376. [CrossRef]
12. Lee, H.M.; Heo, Y.J.; An, K.H.; Jung, S.C.; Chung, D.C.; Park, S.J.; Kim, B.J. A study on optimal pore range for high pressure hydrogen storage behaviors by porous hard carbon materials prepared from a polymeric precursor. *Int. J. Hydrogen Energy* **2018**, *43*, 5894–5902. [CrossRef]
13. Rosi, N.L.; Eckert, J.; Eddaoudi, M.; Vodak, D.T.; Kim, J.; O'Keeffe, M.; Yaghi, O.M. Hydrogen storage in microporous metal-organic frameworks. *Science* **2003**, *300*, 1127–1129. [CrossRef]

14. Mohan, M.; Sharma, V.K.; Kumar, E.A.; Gayathri, V. Hydrogen storage in carbon materials—A review. *Energy Storage* **2019**, *1*, e35. [CrossRef]
15. Barghi, S.H.; Tsotsis, T.T.; Sahimi, M. Chemisorption, physisorption and hysteresis during hydrogen storage in carbon nanotubes. *Int. J. Hydrogen Energy* **2014**, *39*, 1390–1397. [CrossRef]
16. Lee, S.-Y.; Yop Rhee, K.; Nahm, S.-H.; Park, S.-J. Effect of p-type multi-walled carbon nanotubes for improving hydrogen storage behaviors. *J. Solid State Chem.* **2014**, *210*, 256–260. [CrossRef]
17. Ahmed, A.; Seth, S.; Purewal, J.; Wong-Foy, A.G.; Veenstra, M.; Matzger, A.J.; Siegel, D.J. Exceptional hydrogen storage achieved by screening nearly half a million metal-organic frameworks. *Nat. Commun.* **2019**, *10*, 1568. [CrossRef]
18. Xiang, Z.; Cao, D.; Shao, X.; Wang, W.; Zhang, J.; Wu, W. Facile preparation of high-capacity hydrogen storage metal-organic frameworks: A combination of microwave-assisted solvothermal synthesis and supercritical activation. *Chem. Eng. Sci.* **2010**, *65*, 3140–3146. [CrossRef]
19. Hu, Y.H.; Zhang, L. Hydrogen Storage in Metal–Organic Frameworks. *Adv. Mater.* **2010**, *22*, E117–E130. [CrossRef] [PubMed]
20. Lin, K.S.; Adhikari, A.K.; Ku, C.N.; Chiang, C.L.; Kuo, H. Synthesis and characterization of porous HKUST-1 metal organic frameworks for hydrogen storage. *Int. J. Hydrogen Energy* **2012**, *37*, 13865–13871. [CrossRef]
21. Wu, H.; Zhou, W.; Yildirim, T. Hydrogen Storage in a Prototypical Zeolitic Imidazolate Framework-8. *J. Am. Chem. Soc.* **2007**, *129*, 5314–5315. [CrossRef] [PubMed]
22. Férey, G.; Latroche, M.; Serre, C.; Millange, F.; Loiseau, T.; Percheron-Guégan, A. Hydrogen adsorption in the nanoporous metal-benzenedicarboxylate M(OH)(O_2C–C_6H_4–CO_2) (M = Al^{3+}, Cr^{3+}), MIL-53. *Chem. Commun.* **2003**, 2976–2977. [CrossRef]
23. Arean, C.O.; Manoilova, O.V.; Bonelli, B.; Delgado, M.R.; Palomino, G.T.; Garrone, E. Thermodynamics of hydrogen adsorption on the zeolite Li-ZSM-5. *Chem. Phys. Lett.* **2003**, *370*, 631–635. [CrossRef]
24. Dresselhaus, M.S.; Williams, K.A.; Eklund, P.C. Hydrogen Adsorption in Carbon Materials. *MRS Bull.* **1999**, *24*, 45–50. [CrossRef]
25. Figueroa-Torres, M.Z.; Domínguez-Ríos, C.; Cabañas-Moreno, J.G.; Vega-Becerra, O.; Aguilar-Elguézabal, A. The synthesis of Ni-activated carbon nanocomposites via electroless deposition without a surface pretreatment as potential hydrogen storage materials. *Int. J. Hydrogen Energy* **2012**, *37*, 10743–10749. [CrossRef]
26. Caturla, F.; Molina-Sabio, M.; Rodríguez-Reinoso, F. Preparation of activated carbon by chemical activation with $ZnCl_2$. *Carbon* **1991**, *29*, 999–1007. [CrossRef]
27. Hayashi, J.i.; Horikawa, T.; Takeda, I.; Muroyama, K.; Nasir Ani, F. Preparing activated carbon from various nutshells by chemical activation with K_2CO_3. *Carbon* **2002**, *40*, 2381–2386. [CrossRef]
28. Wang, J.; Kaskel, S. KOH activation of carbon-based materials for energy storage. *J. Mater. Chem.* **2012**, *22*, 23710–23725. [CrossRef]
29. Maciá-Agulló, J.A.; Moore, B.C.; Cazorla-Amorós, D.; Linares-Solano, A. Activation of coal tar pitch carbon fibres: Physical activation vs. chemical activation. *Carbon* **2004**, *42*, 1367–1370. [CrossRef]
30. Gogotsi, Y.; Dash, R.K.; Yushin, G.; Yildirim, T.; Laudisio, G.; Fischer, J.E. Tailoring of Nanoscale Porosity in Carbide-Derived Carbons for Hydrogen Storage. *J. Am. Chem. Soc.* **2005**, *127*, 16006–16007. [CrossRef] [PubMed]
31. Wróbel-Iwaniec, I.; Díez, N.; Gryglewicz, G. Chitosan-based highly activated carbons for hydrogen storage. *Int. J. Hydrogen Energy* **2015**, *40*, 5788–5796. [CrossRef]
32. Shafeeyan, M.S.; Daud, W.M.A.W.; Houshmand, A.; Shamiri, A. A review on surface modification of activated carbon for carbon dioxide adsorption. *J. Anal. Appl. Pyrolysis* **2010**, *89*, 143–151. [CrossRef]
33. Maulana Kusdhany, M.I.; Lyth, S.M. New insights into hydrogen uptake on porous carbon materials via explainable machine learning. *Carbon* **2021**, *179*, 190–201. [CrossRef]
34. Georgakis, M.; Stavropoulos, G.; Sakellaropoulos, G.P. Molecular dynamics study of hydrogen adsorption in carbonaceous microporous materials and the effect of oxygen functional groups. *Int. J. Hydrogen Energy* **2007**, *32*, 1999–2004. [CrossRef]
35. Agarwal, R.K.; Noh, J.S.; Schwarz, J.A.; Davini, P. Effect of surface acidity of activated carbon on hydrogen storage. *Carbon* **1987**, *25*, 219–226. [CrossRef]
36. Lee, S.-Y.; Park, S.-J. Effect of chemical treatments on hydrogen storage behaviors of multi-walled carbon nanotubes. *Mater. Chem. Phys.* **2010**, *124*, 1011–1014. [CrossRef]
37. Dubinin, M.M.; Astakhov, V.A. Development of the concepts of volume filling of micropores in the adsorption of gases and vapors by microporous adsorbents. *Bull. Acad. Sci. USSR Div. Chem. Sci.* **1971**, *20*, 8–12. [CrossRef]
38. Marinello, S.; Lolli, F.; Gamberini, R.; Rimini, B. A second life for cigarette butts? A review of recycling solutions. *J. Hazard. Mater.* **2020**, *384*, 121245. [CrossRef] [PubMed]
39. Blankenship, L.S.; Mokaya, R. Cigarette butt-derived carbons have ultra-high surface area and unprecedented hydrogen storage capacity. *Energy Environ. Sci.* **2017**, *10*, 2552–2562. [CrossRef]
40. Blankenship, T.S., II; Balahmar, N.; Mokaya, R. Oxygen-rich microporous carbons with exceptional hydrogen storage capacity. *Nat. Commun.* **2017**, *8*, 1545. [CrossRef]
41. González-García, P. Activated carbon from lignocellulosics precursors: A review of the synthesis methods, characterization techniques and applications. *Renew. Sustain. Energy Rev.* **2018**, *82*, 1393–1414. [CrossRef]
42. Baek, J.; Lee, H.-M.; Roh, J.-S.; Lee, H.-S.; Kang, H.S.; Kim, B.-J. Studies on preparation and applications of polymeric precursor-based activated hard carbons: I. Activation mechanism and microstructure analyses. *Microporous Mesoporous Mater.* **2016**, *219*, 258–264. [CrossRef]

43. Heo, Y.-J.; Park, S.-J. Synthesis of activated carbon derived from rice husks for improving hydrogen storage capacity. *J. Ind. Eng. Chem.* **2015**, *31*, 330–334. [CrossRef]
44. Sevilla, M.; Fuertes, A.B.; Mokaya, R. High density hydrogen storage in superactivated carbons from hydrothermally carbonized renewable organic materials. *Energy Environ. Sci.* **2011**, *4*, 1400–1410. [CrossRef]
45. Sevilla, M.; Mokaya, R. Energy storage applications of activated carbons: Supercapacitors and hydrogen storage. *Energy Environ. Sci.* **2014**, *7*, 1250–1280. [CrossRef]
46. Jain, A.; Balasubramanian, R.; Srinivasan, M.P. Hydrothermal conversion of biomass waste to activated carbon with high porosity: A review. *Chem. Eng. J.* **2016**, *283*, 789–805. [CrossRef]
47. Bedin, K.C.; Martins, A.C.; Cazetta, A.L.; Pezoti, O.; Almeida, V.C. KOH-activated carbon prepared from sucrose spherical carbon: Adsorption equilibrium, kinetic and thermodynamic studies for Methylene Blue removal. *Chem. Eng. J.* **2016**, *286*, 476–484. [CrossRef]
48. Sevilla, M.; Fuertes, A.B. The production of carbon materials by hydrothermal carbonization of cellulose. *Carbon* **2009**, *47*, 2281–2289. [CrossRef]
49. Yan, X.; Jia, Y.; Chen, J.; Zhu, Z.; Yao, X. Defective-Activated-Carbon-Supported Mn–Co Nanoparticles as a Highly Efficient Electrocatalyst for Oxygen Reduction. *Adv. Mater.* **2016**, *28*, 8771–8778. [CrossRef]
50. Heo, Y.-J.; Seong, D.B.; Park, S.-J. Synthesis of polyethylenimine-impregnated titanate nanotubes for CO_2 capture: Influence of porosity and nitrogen content on amine-modified adsorbents. *J. CO2 Util.* **2019**, *34*, 472–478. [CrossRef]
51. Thommes, M.; Kaneko, K.; Neimark, A.V.; Olivier, J.P.; Rodriguez-Reinoso, F.; Rouquerol, J.; Sing, K.S.W. Physisorption of gases, with special reference to the evaluation of surface area and pore size distribution (IUPAC Technical Report). *Pure Appl. Chem.* **2015**, *87*, 1051–1069. [CrossRef]
52. Lee, S.-Y.; Park, S.-J. Effect of temperature on activated carbon nanotubes for hydrogen storage behaviors. *Int. J. Hydrogen Energy* **2010**, *35*, 6757–6762. [CrossRef]
53. Ramirez-Vidal, P.; Canevesi, R.L.S.; Sdanghi, G.; Schaefer, S.; Maranzana, G.; Celzard, A.; Fierro, V. A Step Forward in Understanding the Hydrogen Adsorption and Compression on Activated Carbons. *ACS Appl. Mater. Interfaces* **2021**, *13*, 12562–12574. [CrossRef]
54. Fairen-Jimenez, D.; Colón, Y.J.; Farha, O.K.; Bae, Y.-S.; Hupp, J.T.; Snurr, R.Q. Understanding excess uptake maxima for hydrogen adsorption isotherms in frameworks with rht topology. *Chem. Commun.* **2012**, *48*, 10496–10498. [CrossRef]
55. Masika, E.; Mokaya, R. Preparation of ultrahigh surface area porous carbons templated using zeolite 13X for enhanced hydrogen storage. *Prog. Nat. Sci. Mater. Int.* **2013**, *23*, 308–316. [CrossRef]
56. Poirier, E.; Chahine, R.; Bose, T.K. Hydrogen adsorption in carbon nanostructures. *Int. J. Hydrogen Energy* **2001**, *26*, 831–835. [CrossRef]
57. Balahmar, N.; Mokaya, R. Pre-mixed precursors for modulating the porosity of carbons for enhanced hydrogen storage: Towards predicting the activation behaviour of carbonaceous matter. *J. Mater. Chem. A* **2019**, *7*, 17466–17479. [CrossRef]
58. Attia, N.F.; Jung, M.; Park, J.; Jang, H.; Lee, K.; Oh, H. Flexible nanoporous activated carbon cloth for achieving high H_2, CH_4, and CO_2 storage capacities and selective CO_2/CH_4 separation. *Chem. Eng. J.* **2020**, *379*, 122367. [CrossRef]
59. Rossetti, I.; Ramis, G.; Gallo, A.; Di Michele, A. Hydrogen storage over metal-doped activated carbon. *Int. J. Hydrogen Energy* **2015**, *40*, 7609–7616. [CrossRef]
60. Wang, H.; Gao, Q.; Hu, J.; Chen, Z. High performance of nanoporous carbon in cryogenic hydrogen storage and electrochemical capacitance. *Carbon* **2009**, *47*, 2259–2268. [CrossRef]
61. Sangchoom, W.; Mokaya, R. Valorization of Lignin Waste: Carbons from Hydrothermal Carbonization of Renewable Lignin as Superior Sorbents for CO_2 and Hydrogen Storage. *ACS Sustain. Chem. Eng.* **2015**, *3*, 1658–1667. [CrossRef]
62. Yang, Z.; Xia, Y.; Mokaya, R. Enhanced Hydrogen Storage Capacity of High Surface Area Zeolite-like Carbon Materials. *J. Am. Chem. Soc.* **2007**, *129*, 1673–1679. [CrossRef] [PubMed]
63. Lee, S.-Y.; Park, S.-J. Influence of oxygen-functional groups on carbon replicas for hydrogen adsorption. *Phys. Status Solidi* **2012**, *209*, 694–697. [CrossRef]
64. Lee, S.-Y.; Park, S.-J. Influence of the pore size in multi-walled carbon nanotubes on the hydrogen storage behaviors. *J. Solid State Chem.* **2012**, *194*, 307–312. [CrossRef]